Applied Thermal Engineering 128 (2018) 1186–1195

Contents lists available at ScienceDirect

Applied Thermal Engineering

journal homepage: www.elsevier.com/locate/apthermeng

Research Paper

Thermal oxidation coking of aviation kerosene RP-3 at supercritical pressure in helical tubes

Yanchen Fu, Guoqiang Xu, Jie Wen *, Haoran Huang

National Key Laboratory of Science and Technology on Aero-Engine Aero-thermodynamics, Collaborative Innovation Center for Advanced Aero-Engine, School of Energy and Power Engineering, Beihang University, Beijing 100191, China

HIGHLIGHTS

- Thermal oxidation coking amount distribution is more uniform in helical tubes.
- Smaller helical diameter makes the coking peak closer to the flow downstream.
- The total coking amount sharply decreased with the increase of helical coil numbers.
- Three coking morphologies and various elements distributions are detected.

ARTICLE INFO

Article history:
Received 12 June 2017
Revised 3 September 2017
Accepted 20 September 2017
Available online 21 September 2017

Keywords:
Thermal oxidation coking
Supercritical RP-3
Helical tubes
SEM
Coking elements

ABSTRACT

The mechanism of thermal oxidation coking of aviation kerosene RP-3 at a supercritical pressure of 5 MPa in helical tubes was analyzed. The bulk temperature of the fuel was varied from 400 K to 723 K, and the mass flux was varied from 393 kg/m^2 s to 1178 kg/m^2 s. Four types of helical tubes with different helical diameters were bent and tested for a maximum duration of 5 h. The total coking amount and distribution were analyzed using weighing method, and the standard error was less than 0.07 mg. The results indicate that coking distribution is more uniform than in the case of a straight tube, and that there is no prominent coking peak because of the effect of centrifugal force. The maximum total coking amount among all the experiments decreased by approximately 69.5% compared with that in a straight tube. Through measurements performed using a scanning electron microscope, three main types of coking morphologies were observed: thin coking layer, dense clumps, and crystalline particles. Moreover, various types of coking elements were detected under different working conditions.

1. Introduction

In the cooled cooling air (CCA) technology [1], aviation kerosene can be used as the cooling medium that flows inside the heat exchanger tubes to provide a high heat capacity. As the pumping system for the hydrocarbon fuel is approximately 3.45–6.89 MPa in typical aero-engines [2], the hydrocarbon fuel will be under supercritical pressure during the heating process. According to previous researches [3–5], thermal coking deposition occurs when the bulk temperature is higher than 163 °C. The hydrocarbon molecules in the fuel react with dissolved oxygen to cause thermal oxidation coking in the temperature range of 163–450 °C. However, thermal pyrolysis deposition becomes the dominant reaction when the temperature is higher than 450 °C. The coke depositing on the inner surface of the tube will decrease the heat transfer between the aviation kerosene and cooling air. Furthermore, a certain mass of coke can block the combustion nozzle or heat exchanger tube and trigger an aero-engine accident.

Thermal coking of hydrocarbon fuel at supercritical pressures involves complicated physical and chemical reactions [6]. Many factors influence the coking process, such as bulk temperature, experimental time, dissolved oxygen concentration, and tube material. Marteney [7] and Hazllet [8] considered that bulk temperature is the most important factor that affects thermal oxidation coking, and that temperature directly determines the intensity of the coking process. The results show that coking deposition and colloid are not formed when the fuel temperature is lower than 150 °C. The coking rate increases with temperature, and reaches the peak level at a temperature of approximately 316 °C. This peak appears because of the coupling effect between temperature and dissolved oxygen [9], as the variations in these two factors produce opposite effects. The hydrocarbon fuel coking shows

* Corresponding author.
E-mail address: wenjie@buaa.edu.cn (J. Wen).

https://doi.org/10.1016/j.applthermaleng.2017.09.101
1359-4311/

different characteristics depending on the conditions of the coking experiments. Jones et al. [10,11] studied supercritical Jet-A thermal oxidation coking under different experimental durations, and found that the coking rate is mainly affected by the rate of consumption of dissolved oxygen in an experiment with 6 h duration. However, it was found that the coking rate decreases continuously as the metal surface is covered by coking in the experiment with 70 h duration. Hazlett [12,13] suggested that the porous medium formed during the coking process can enhance the contact surface area between the inner wall and the fuel. Furthermore, the porous structure on the coking surface can retain the fuel on the high temperature wall and increase the reaction time [14], which can enhance the adhesion ability of the surface coking. Later, Eser et al. [15] applied various types of metal coatings on AISI 304 and studied their effects on the inhibition of carbon deposition during thermal oxidative degradation of jet fuel. It was reported that coking inhibition effect is related to the acidity level of the oxygenated intermediates during thermal stressing with the coating surfaces.

Many researchers have studied thermal coking of Chinese aviation kerosene RP-3, the most popular jet fuel in China, with critical pressure and temperature of 2.319 MPa and 372.2 °C, respectively. Xu et al. [16,17] experimentally investigated the influence of various physical and chemical factors on thermal oxidation in vertical tubes, and evaluated different methods for coking inhibition. Besides, an additive named BHTD-E50D was developed to suppress thermal oxidation coking; by using this additive, the amount of coking deposition on the inner wall surface decreased by 73.5%. In recent research, Zhu et al. [18] studied the thermal oxidation coking in tubes having different surface treatments and concluded that electrolytically passivated treatments could reduce the total coking deposition by approximately 58.3% and 35.8% compared with untreated tubes. To simulate the actual working conditions, Tao et al. [19,20] experimentally studied the effect of vibration on thermal oxidation coking of hydrocarbon fuel at supercritical pressures. The results showed that vibration could make the coking distribution more uniform and extend the tube-blocking time.

Most of the research work to date focused on the thermal oxidation coking in straight stainless steel tubes [21–23]. However, compact heat exchangers consist of a series of curved tubes in actual applications of the CCA technology. In previous research, the investigations conducted on fluid characteristics in curved tubes were mainly concerned with the effects of tube geometry on heat transfer [24–26] and resistance to flow [27,28]. In several

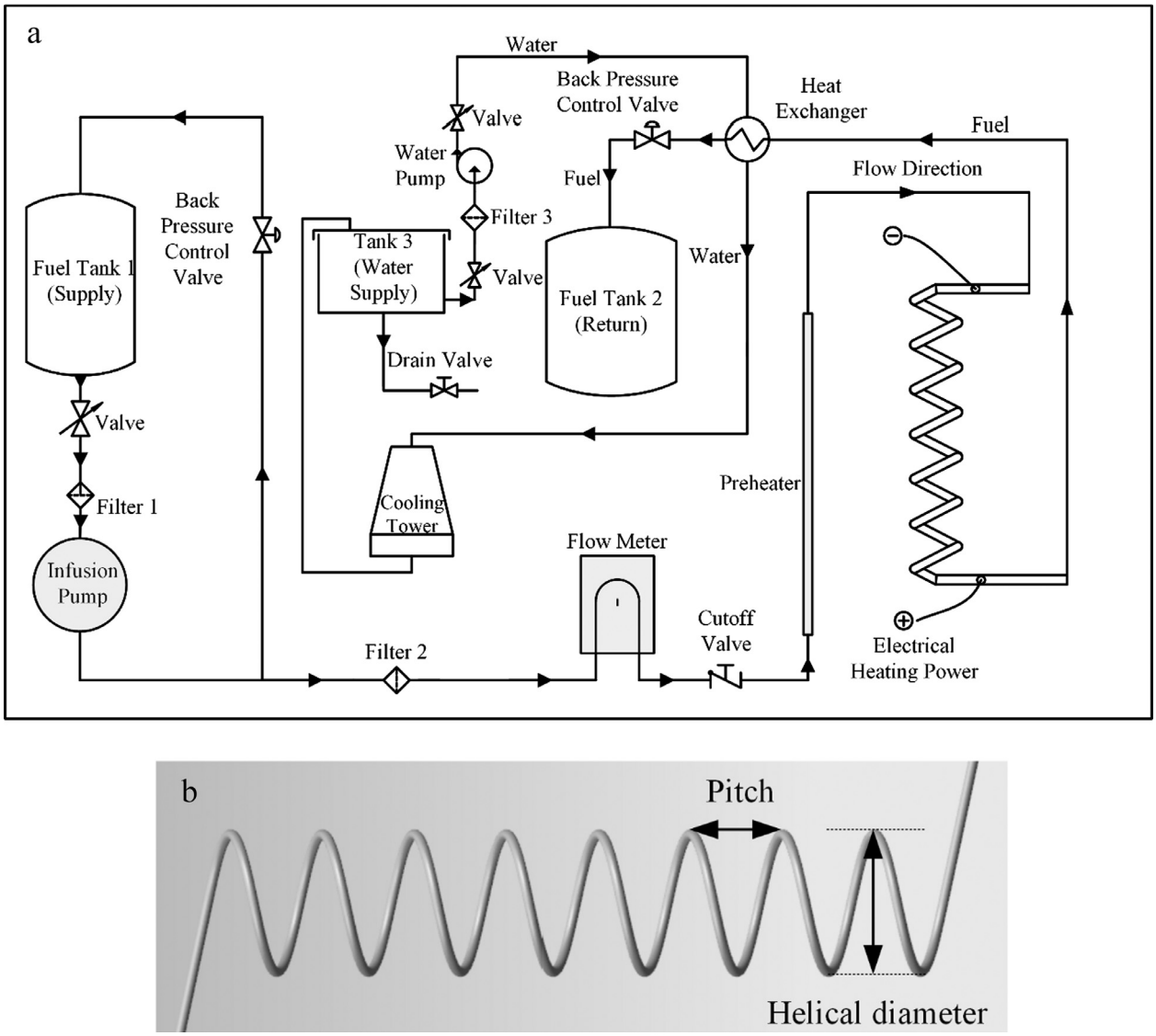

Fig. 1. Schematics of supercritical hydrocarbon fuel coking system (a) and helical tube (b).

Table 1
Experimental tube parameters.

Straight tube		Helical tube				
Inner diameter (mm)	1.82	Type	A	B	C	D
		Pitch (mm)	40			
		Helical diameter (mm)	502	118	67	46
Outer diameter (mm)	2.20	Single coil length (mm)	1500	372.9	214.3	149.9
		Coil numbers	1	4	7	10
Total length (mm)	1500	Helix angle	1.5	6.2	10.8	15.5
		Helical length (mm)	1500			
		Total length (mm)	1800			

studies, the investigators presented various correlations and only limited studies have been conducted on thermal coking of hydrocarbon fuel in curved tubes. Recently, Hou [29] studied the thermal stability characteristics of aviation kerosene flowing through a heated S-tube; the results show that sudden changes in the wall temperature, together with temperature gradients, promote large coking deposition on the surface. Based on measurement data of thermal properties [30–33], thermal oxidation coking depositions for aviation kerosene RP-3 at supercritical pressures in helical tubes were experimentally evaluated in this study. The effects of physical factors on the distribution of coking in various helical tubes were compared with those in straight tubes, and the coking characteristics under the action of centrifugal force were analyzed.

2. Method and procedure

2.1. Experimental system

Fig. 1a shows the experimental system for the study of flow and heat transfer of supercritical hydrocarbon fuel. This system consists of a preheat section, a test section, a data acquisition section, and a recycling system. The system can supply fuel with mass flow rate in the range of 0.1–8.33 g/s, apply system pressure in the range of 0.1–10 MPa, and deliver a maximum heat power of 60 kW; these ranges cover all the test conditions. The hydrocarbon fuel was supplied from a fuel tank; it was passed through a filter screen to avoid blockage of the fuel path. The infusion pump (SP6015, 15 MPa, 0.01–600 mL/min) could keep the system in a stable pressure condition; it had a provision to relieve excess pressure automatically to keep the system safe. The main path preparative fuel was then pumped to the preheated and test sections. The mass flux was controlled by the pump, and was measured by a Coriolis mass flow meter (DMF-1-1, accuracy: 0.15%). Two sets of power supply (TN-KGZ01, 100 V, 200 A) were used to heat the pressurized path to achieve the required temperature of the test section. After flowing through the test section, the high temperature fuel was cooled to 30 °C using a tube and shell water cooler, and then passed into the waste fuel tank. A back-pressure valve was set behind the cooler to regulate the system pressure in the range of 0.1–6 MPa. Moreover, the set-up had instruments for measuring the differential pressure, temperature, heating voltage, and current. All the data were acquired as electrical signals through ADAM-4018 data logger; the data were recorded and stored on a computer using ADAM-4520 converter.

2.2. Test section

The helical tubes for the experiments were prepared by bending 1800 mm long stainless steel straight tubes having an inner diameter of 1.82 mm and an outer diameter of 2.2 mm. Thermal insulation sections, each 150 mm long, were provided both in the inlet and outlet sections, and the 1500 mm long section in the middle was the experimental section which was subjected to heating. To evaluate the effect of bending diameter on the coking characteristics, four types of helical tubes with the same pitch were manufactured. The schematic of the helical tubes is shown in Fig. 1b, and the detailed parameters of the straight and helical tubes are listed in Table 1. The experimental section was connected to the system by a special silver weld joint to reduce the local resistance to the flow of current. There were 15 NiCr-NiSi thermocouples mounted with uniform spacing on the surface of the helical tubes to monitor the variation in the tube surface temperature. Further, to maintain consistency, each thermocouple was mounted on the outer side of the tubes in the circumferential direction to measure the wall temperature. The entire test section was covered with Aspen thermal insulation material to reduce heat loss.

Table 2
Experimental conditions.

System pressure (MPa)	5
Mass flux (kg/m^2 s)	393–1178
Inlet temperature (K)	400
Outlet temperature (K)	700–723
Duration time (h)	1–5

As presented in Table 2, the system pressure was set to 5 MPa, and the inlet fuel temperature was kept constant at 400 K. The outlet temperature and duration were 723 K and 5 h (maximum), respectively. To ensure that there is sufficient oxygen for the coking reaction during the experiment, oxygen was filled for 30 min in the fuel tank before each experiment; this ensured the presence of dissolved oxygen in a saturated state with a concentration of approximately 30 ppm [34].

2.3. Weighing method and uncertainty analysis

As the duration of the experiments on the helical tube is limited, the coking amount will be of the order of several milligrams. Quartz microbalance measurement method [35], charcoal burning method [36,37], and weighing method are the three common methods used to measure the coking amount. Based on the results of previous research and considering higher accuracy requirement, weighing method was adopted in this study. The first three steps in the experiment were as follows: cut the experimental tube uniformly into several segments of size 5 cm, dry in the furnace at 120 °C for 1 h, and make the first weighing using a standard analytical balance (Sartorius BT224S, Germany) with a resolution of 0.1 mg. The fourth step was to perform ultrasonic cleaning of the segments for 3 h using an alkaline cleaning fluid, and then clean both inside and outside of the tube segments by rinsing in hydrous ethanol. The last two steps were to dry the segments in the furnace at 100 °C and weigh them again after drying. Thus, the coking amount for every segment was obtained by the difference between the initial and final weights. To study the coking characteristics for various helical diameters and deeply analyze the mechanism of

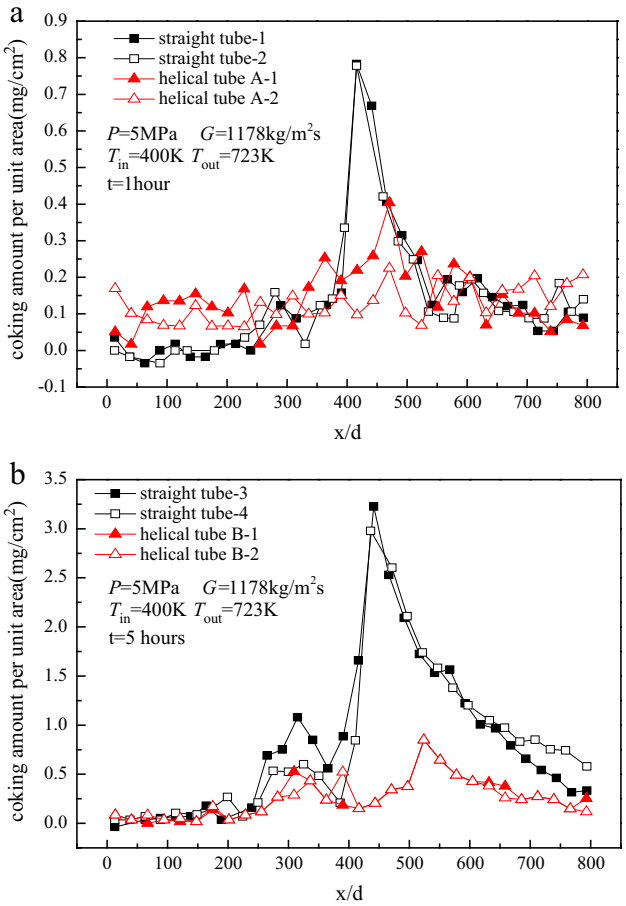

Fig. 2. Repetitive evaluation of coking amount per unit area distributions for 1 h (a) and 5 h (b) experiments.

thermal oxidation coking formation, the coking morphologies and element distributions were observed using an SEM (scanning electron microscope) and EDS (energy dispersive spectrometer); JCM-6000Plus from Bench-top, Japan, was used for this purpose.

The coking amount in each segment can be obtained using the following equation.

$$m(i) = m_1(i) - m_2(i) \tag{1}$$

where i represents the number of the segment; m_1 (i) and m_2 (i) are the weights before and after ultrasonic cleaning, respectively. The total coking amount can be obtained from Eq. (2).

$$m = \sum_{i=1}^{n} m(i) = \sum_{i=1}^{n} [m_1(i) - m_2(i)] \tag{2}$$

According to the error transfer formula, the standard error in the measurement of coking amount in each segment and the total coking amount can be calculated using Eq. (3) and Eq. (4), respectively.

$$\Delta m(i) = \sqrt{(\Delta m_1(i))^2 + (\Delta m_2(i))^2} \tag{3}$$

$$\Delta m = \sqrt{\sum_{i=1}^{n} (\Delta m(i))^2} \tag{4}$$

The error in the value of coking amount in each segment is obtained as ±0.07 mg based on the errors in the measurement of tube length, inner diameter, and weights (using the analytical balance). Thus, the absolute error for the total coking amount is obtained as ±0.38 mg, calculated using Eq. (4). However, the coking

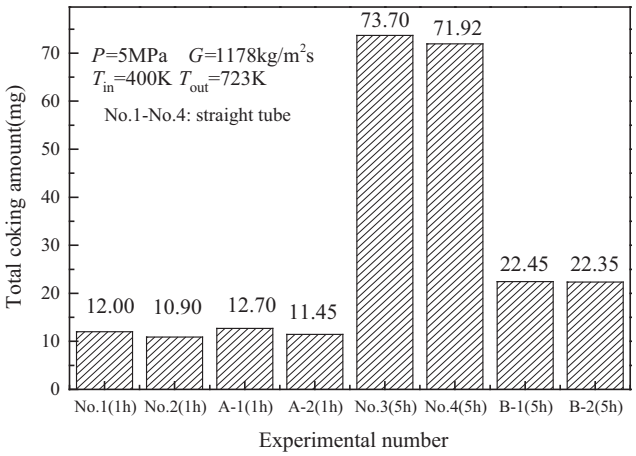

Fig. 3. Total coking amount comparison between 1 h and 5 h experiments.

amount per unit area is to be used as the reference value, since there could be variations in the lengths of different segments during the cutting process; this is calculated using Eq. (5).

$$\overline{\Delta m}(i) = \Delta m(i)/A = \Delta m(i)/(\pi d_{in} L(i)) \tag{5}$$

Further, 10 segments of size 5 cm are cut and weighed. The average weight of one segment is denoted as $\bar{m}_0$. Hence, the accurate value of the length of each segment can be obtained using Eq. (6), and the absolute error for the coking amount per unit area is obtained as ±0.07 mg/cm^2.

$$L(i) = \frac{m_2(i)}{\bar{m}_0} \tag{6}$$

3. Results and discussion

3.1. System verification

To verify the accuracy and repeatability of the hydrocarbon fuel coking experimental system, the experiments on straight tube and helical tubes A and B for 1 h and 5 h durations have been conducted in two groups. The experimental parameters and their values are as follows: system pressure of 5 MPa, mass flux of 1178 kg/m^2 s, inlet temperature of 400 K, and outlet temperature of 723 K. The distribution of coking amount per unit area along the test tube and the total coking amount are shown in Figs. 2 and 3, respectively. In the figures, x/d is the dimensionless position; x and d are the tube length from the heating point and tube diameter, respectively. The results show that both coking distribution and total amount have good repeatability in both the experiments. For the straight tube, the deviations in the total coking amount in the experiments with 1 h and 5 h durations are 9.6% and 2.4%, respectively. The corresponding deviations for helical tubes A and B are 9.8% and 0.5%, respectively. The coking distribution curves almost coincide for the two groups.

Fig. 2a shows the coking distribution for 1 h duration in helical tube A. As the bulk flow in the single-coil tube is influenced by the relatively small centrifugal force, the coking adhesion on the tube surface is distributed more uniformly along the tube, and there is no prominent coking peak. In addition, the coking amount in helical tube B has decreased by 69.5% compared with that in the straight tube, as shown in Fig. 2b. The experiments conducted on helical tubes for 1 h and 5 h durations show that the coking peak could be inhibited irrespective of the number of coils. There are two main reasons for the decrease in coking amount in the helical tubes: the effect of centrifugal force and increase in heat transfer.

As the fluid in the central part moves to the outer side and the fluid near the wall moves to the inner side, secondary flow is induced, resulting in an increase in the intensity of turbulence and a decrease in the laminar sub-layer where the coking deposition occurs. Further, the centrifugal force may lead to higher heat transfer, and hence decrease the wall temperature because of the effect of large secondary flow [38,39]. Thus, the coking deposition on the surface could be inhibited by the strong interaction between the centrifugal force and temperature variations.

3.2. Effects of outlet temperature and duration

The formation of thermal oxidation coke deposits at supercritical pressures is the result of free radical chain reactions between the hydrocarbon fuel molecules and dissolved oxygen molecules. Coking precursors are transferred to the surface to form the coking deposits through a series of complicated physical and chemical reactions. The wall and bulk temperature distributions are the main factors that influence coking distribution. Tevelde and Glickstein [40] concluded that wall temperature plays a leading role in thermal oxidation coking based on research conducted on four types of hydrocarbon fuels. However, the research by Chin and Lefevre [41] shows that bulk temperature is the key factor. According to previous research on coking in straight tubes [19], the coking peak appears in the temperature range of 572–586 K under various conditions of inlet temperatures and mass fluxes, and the wall temperature varies significantly under different conditions. These phenomena reflect the influence of bulk temperature on thermal coking of aviation kerosene RP-3 in straight tubes. The thermal oxidation coking distributions with inner wall and bulk temperature variations at outlet temperatures of 700 K and 723 K, respectively, in helical tube A are shown in Fig. 4. The local bulk temperature of the fuel is determined by the energy balance relationship among the local heat flux and the inlet and outlet fuel enthalpies, which have been measured in previous studies [42]. The inner wall temperature is determined by solving the one-dimensional thermal conductivity equation under the cylindrical coordinates system using the measured data of outer wall temperatures [43]. It can be seen that more coking deposition is formed in the later part in the helical tube when the outlet temperature is 723 K. When the dimensionless position x/d lies between 470 and 793, the coking amount at the outlet temperature of 723 K is 49.8% more than that at 700 K. In addition, at 700 K, the coking peak occurs at the position x/d = 524.2, corresponding to the bulk temperature of 629.1 K. However, the coking peak at 723 K corresponds to the bulk temperature of 596.3 K at the position x/d = 470.4. Thus, the coking peak moves toward the higher bulk temperature region, as the higher bulk temperature can accelerate the coking reaction and deposition. This further confirms that bulk temperature is the key factor that influences the coking distribution. Furthermore, the coking distribution shows that coking at the entry and exit are almost consistent; this confirms that adequate duration can ensure complete thermal oxidation coking. As shown in Fig. 5, the higher outlet temperature is caused by the larger heat flux and this results in a strong secondary flow. The reason is that the higher heat flux decreases the local fuel density and induces higher thermal acceleration. Hence, the coking amount is no longer directly proportional to the duration, and the influence of wall temperature becomes more significant.

The level of wall coking deposition is also determined by the capacity to transport the coking reactants and products from the mainstream area to the static layer near the wall. The mass flux can influence the Reynolds number of the mainstream flow and can thus affect the mass transport of the coking reactants. The influence of the mass flow rate on the coking distribution in helical tube C is shown in Fig. 6. It can be seen that the coking peak moves toward the downstream side of the tube with the increase in mass flux. As the outlet temperature remains constant under various conditions, the mainstream flow has a much larger capacity to carry the dissolved oxygen, and the range of wall coking deposition is wider for the larger mass flux condition. Thus, the coking peak position moves from the dimensionless position x/d = 200 to x/d = 530.

In a helical tube with a constant pitch, the critical Reynolds number that distinguishes between laminar and turbulent flows is defined by the Schmidt [44] equation.

$$\mathrm{Re}_c = 2300\left[1 + 8.6\left(\frac{d}{D}\right)^{0.45}\right] \tag{7}$$

For helical tube C, the critical Reynolds number is approximately 7200, and is shown as a horizontal line in Fig.6a. Most of the flow in the low mass flux condition (G = 393 kg/m^2 s) is in the laminar state, and the coking rate is larger than in the other conditions at the same location. The reason is that the lower flow velocity leads to heat deterioration, and the higher wall temperature promotes adherence of the coking precursor to the inner surface; thus, the coking micelles would not be transported downstream quickly to form coking deposition. Furthermore, at the dimensionless position x/d < 420, there is no prominent coking peak, because the large consumption of dissolved oxygen in the

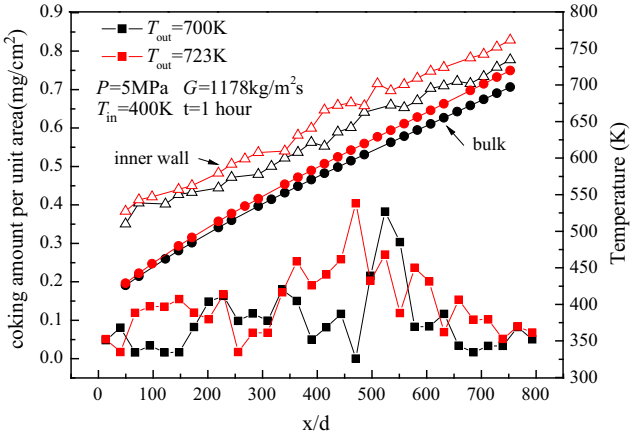

Fig. 4. Outlet temperature influences on coking distribution in helical tube A.

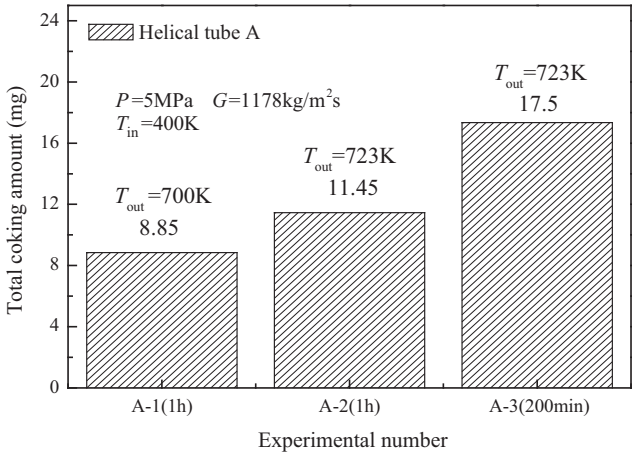

Fig. 5. Outlet temperature and duration time influences on the total coking amount in helical tube A.

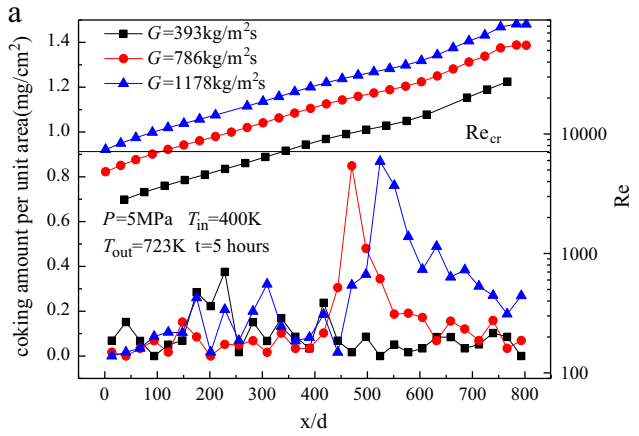

Fig. 6. Mass flow rate influences on the coking distribution in helical tube C.

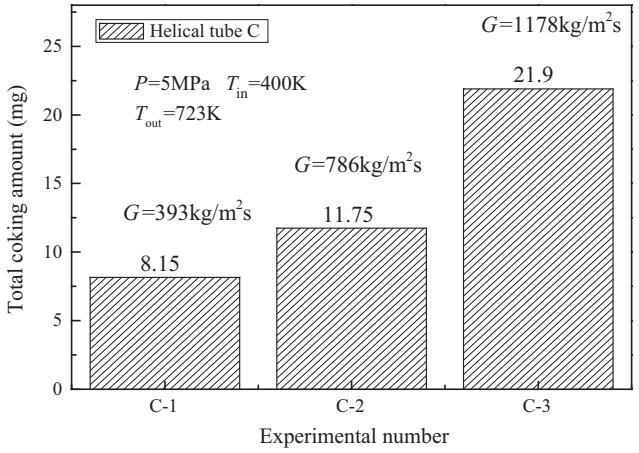

Fig. 7. Mass flow rate influences on the total coking amount in helical tube C.

first half of the tube leads to a decrease in the coking amount per unit area. Fig.6b shows the inner wall temperature variations along the tube at the beginning and end of the experiments. As the bulk temperature variations for different mass flow rates are identical, they are not shown in the figure. It can be seen that the maximum wall temperature occurs at the coking peak when the mass flow rate is 1178 kg/m^2 s. There are minor changes in the wall temperature at the other dimensionless positions when the mass flow rates are 393 kg/m^2 s and 786 kg/m^2 s. These phenomena could also match the velocity explanation on the surface coking deposition. Fig. 7 shows the variation in the total coking amount under

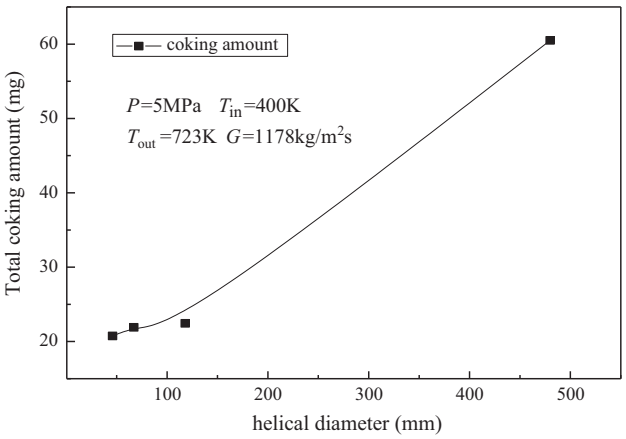

Fig. 8. Helical diameter influences on the total coking amount.

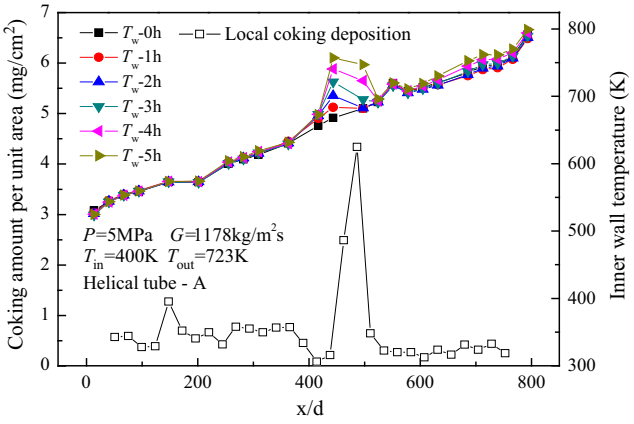

Fig. 9. Coking amount and inner wall temperature distributions in helical tube A.

different mass flux values; it can be seen that the coking amount per unit area increases with the increase in mass flux. As the larger mass flux causes more fuel to participate in the thermal oxidation coking reaction, it can lead to the production of larger amount of coking precursor. On the other hand, the centrifugal force will strengthen the flow mixing effect near the wall surface and improve the possibility of coking adhesion on the inner surface. Hence, more thermal oxidation coking occurs with large mass flux. This explains the variation in coking deposition under various conditions.

3.3. Effects of helical diameter

Fig. 8 shows the variation in the total coking amount for helical tubes with different helical diameters. The following conditions were kept constant in the experiments: system pressure of 5 MPa, mass flux of 1178 kg/m^2 s, inlet temperature of 400 K, and outlet temperature of 723 K. It was observed that the total coking amount increases with the increase in helical diameter. As the mass flux value is constant, larger helical diameter results in a decrease in centrifugal acceleration of the mainstream fuel. Then, the decrease in centrifugal force restrains the heat transfer enhancement ability in the same circumferential section. The small temperature gradient near the wall surface promotes the formation of coking deposition and increases the total coking amount. Moreover, the variation in the total coking amount is small for helical tubes with a small diameter, because the centrifugal force

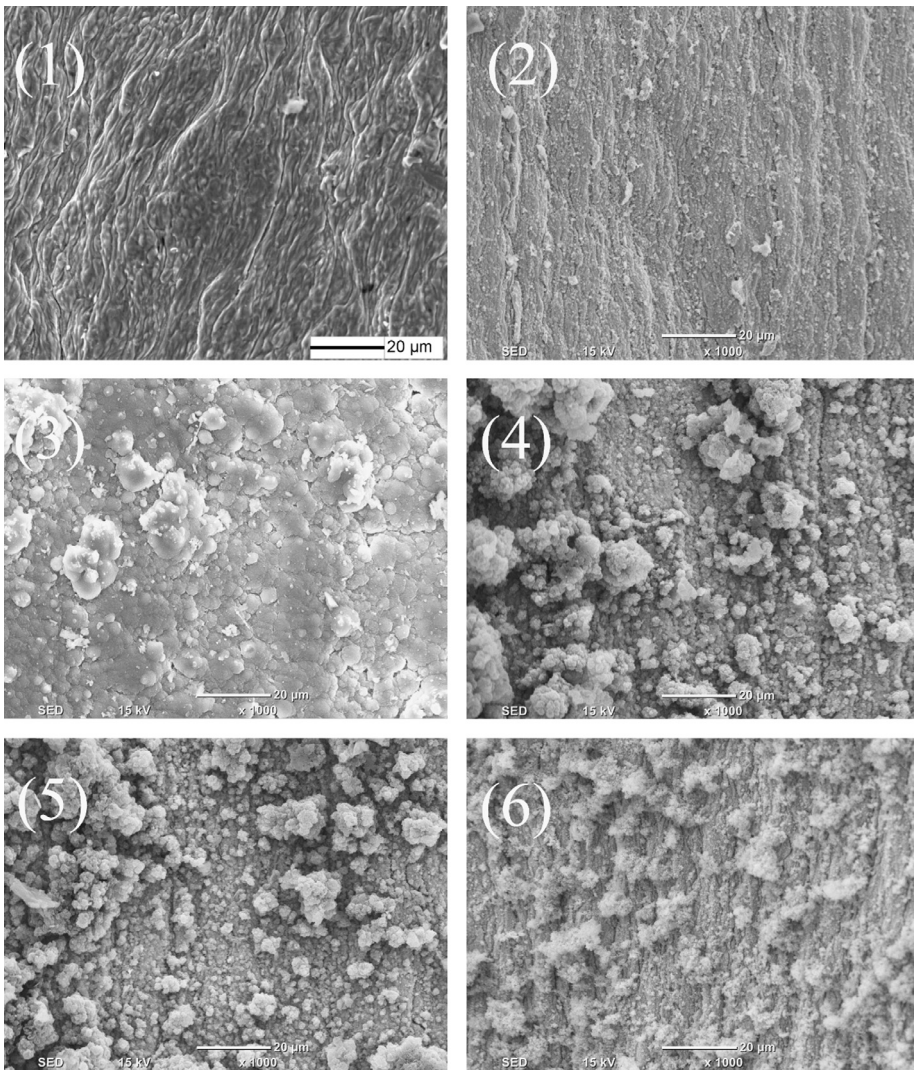

Fig. 10. Inner wall surface coking morphology in helical tube A for various dimensionless positions. (Resolution: ×1000) (1) Bare tube, (2) x/d = 107.5–134.4, (3) x/d = 403.2–430.1, (4) x/d = 457.0–483.9, (5) x/d = 591.4–618.3, (6) x/d = 725.8–752.7.

Table 3
Various elements contents for inner surface coking section in helical tube A.

Mass (%)	A-(1)	A-(2)	A-(3)	A-(4)	A-(5)	A-(6)
C		19.64	82.35	76.95	67.22	49.26
O		16.2	4.6	3.16	5.33	8.91
Fe	71.68	30.53	7.19	9.62	12.69	22.42
Cr	19.36	22.52	2.96	8.56	12.15	8.91
Ni	8.4	2.37	0.58	0.74	0.72	1.53
Al		0.76	2.31			
Si		3.76		0.84	1.07	1.95
S				0.12	0.66	0.75
Mn		2.4				

will have limited influence on flow mixing and the degree of disorder.

To predict the influence of helical diameter on the total coking amount, an empirical equation is derived using the helical curvature parameter (d/D); the empirical equation is given below.

$$M = 2.954\left(\frac{d}{D}\right)^{-0.541} \tag{8}$$

where d represents the tube diameter, and D is the helical diameter. This equation can be used to estimate the thermal oxidation coking amount in compact air-fuel helical tube heat exchangers.

3.4. Thermal coking characteristics

To analyze the coking morphology and the distribution of thermal coking elements, experiments with 5 h duration were conducted in helical tubes A and D. Fig. 9 shows the distribution of inner surface temperatures and coking amount per unit area in helical tube A. It is observed from the figure that the trend of coking distribution is similar to that in a straight tube, and that there is one coking peak along the path. However, the dimensionless position of the coking peak moves to x/d = 480, and the coking amount per unit area is 10 times the value obtained in the

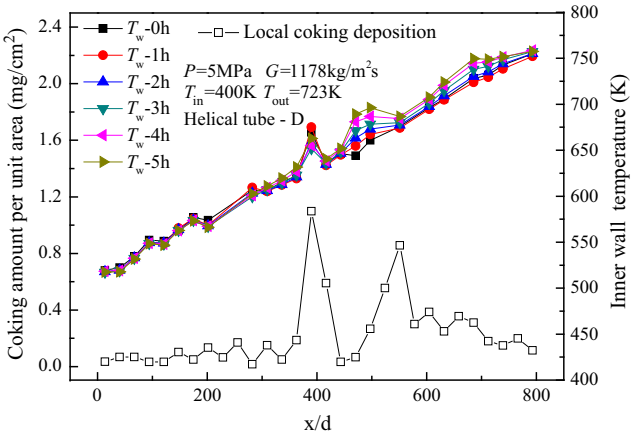

Fig. 11. Coking amount and inner wall temperature distributions in helical tube D.

experiment with 1 h duration. The main flow in the helical tube is influenced by the centrifugal force generated because of the curvature; as a result, the coking distribution becomes more even. Further, the coking amount in the inlet and outlet sections is less, as the temperature is low, and the time is not sufficient for the coking precursor to form deposits on the inner surface. In the position where the coking peak is observed, the inner wall temperature varies from 668 K to 757 K, because the thermal resistance is significantly increased owing to the coking deposition between the tube surface and bulk flow. In the other positions, the inner wall temperature remains steady during the entire experiment, as the coking deposition has little influence on the heat transfer.

Fig. 10 shows the coking morphology at various dimensionless positions before and after the experiment with 5 h duration in helical tube A, and Table 3 presents the mass percentages of the coking elements in the corresponding positions. It can be seen from the figure that the morphological distribution is present in three forms in the dimensionless positions (x/d) between 107.5 and 752.7: thin coking layer (A-2), dense clumps (A-3, A-4), and crystalline particles (A-5, A-6). In the low temperature coking section, the coking ability is too weak to transport the coking precursor, and hence a thin coking layer is formed. The coking precursor mainly consists of alkyl hydro-peroxides produced from the auto-oxidation chain reaction [3]. During this process, the reactant alkane is converted into alkyl hydro-peroxides. Part of the precursor is stripped from the laminar sub-layer under the action of centrifugal force, and the content of element C is approximately 20%. At the dimensionless position x/d between 403.2 and 483.9, where the coking peak occurs, there is accumulation of a certain mass of coking precursor to form dense clumps owing to the wall temperature variation. Hydro-peroxides are chemically unstable, and their molecules are prone to undergo a series of reactions, such as disproportionation, decomposition, and isomerization, resulting in complex products such as aldehydes, acids, and colloids. At higher temperatures, a large amount of insoluble substances, including macromolecular hydrocarbons and other solid particles, separate out from the fluid to form coking deposition on the inner wall.

Because of the centrifugal force resulting from the flow, the coking deposition will be less dense, and it appears as crystalline particles; the content of element C increases to 80%. The content of dissolved oxygen decreases with the ongoing thermal coking reaction, and the content of element Fe dramatically decreases owing to the decrease in the exposed area on the inner wall surface. Behind the dimensionless position corresponding to coking peak A-4, thermal oxidation coking reaches a certain level, and the inner wall temperature is beyond the thermal cracking temperature. However, the thermal resistance due to the coking deposition leads to a lower bulk flow temperature; thus, no cracking phenomenon is observed in this section. At the high temperature section in the outlet, the inner wall temperatures are in the range of 739–799 K, which is far beyond the thermal cracking temperature. Therefore, some level of thermal cracking exists. This reaction is confirmed by the presence of traces of metal sulfides, as

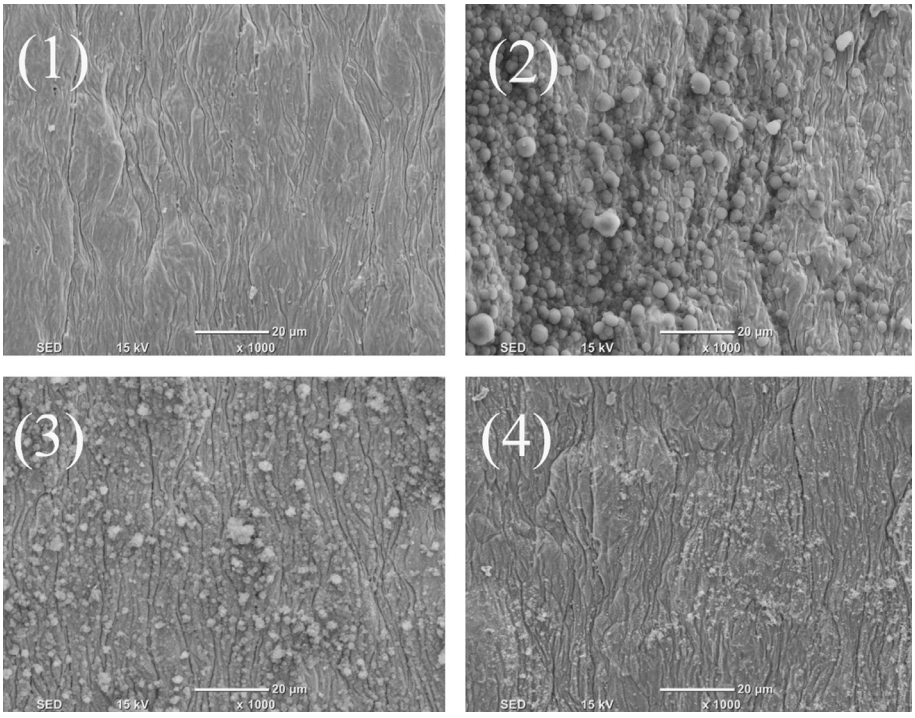

Fig. 12. Inner wall surface coking morphology in helical tube D for various dimensionless positions. (Resolution: ×1000) (1) x/d = 80.6–107.5, (2) x/d = 376.3–403.2, (3) x/d = 537.6–564.5, (4) x/d = 672.0–698.9.

Table 4
Various elements contents for inner surface coking section in helical tube D.

Mass (%)	D-(1)	D-(2)	D-(3)	D-(4)
C	40.2	55.76	86.87	55.05
O	4.16	4.27	1.93	6.39
Fe	31.44	22.21	5.15	18.55
Cr	21.33	15.61	6.05	16.7
Ni	2.22	1.8		1.23
Si	0.65	0.34		0.61
S				0.91

presented in Table 3. This phenomena and explanation are similar to those given in the work by Eser [45] on thermal cracking of hydrocarbon fuels.

Fig. 11 shows the distributions of inner wall temperature and coking amount per unit area with the variation in the dimensionless position in helical tube D. It can be seen that two coking peaks exist at the dimensionless position (x/d) values of 400 and 550. Two peaks are also observed on the inner wall temperature distribution corresponding to the coking peaks, because the thermal resistance due to the coking deposition decreases the heat transfer between the inner wall and fuel bulk flow. The increase in helical laps and centrifugal force accelerate coking adhesion on the inner surface, and lead to major and minor coking peaks. As the precursor concentration reaches the maximum value with high consumption of dissolved oxygen, the local deposit will not be proportional to the precursor concentration. However, the remaining coking precursor would be transported to the downstream side to form the minor coking peak at the inner wall temperature of around 680 K. The thermal oxidation coking morphology for various dimensionless positions is shown in Fig. 12, and the coking element contents are presented in Table 4. Sections D-2 and D-3 correspond to the major and minor coking peaks; D-1 and D-4 represent the low temperature and high temperature sections, respectively. It can be seen from the figure that the coking morphology in the low and high temperature sections is similar to that in helical tube A. Thin, dense coking layers are observed, and the content of element C is approximately 50%, as the inner surface of the tube is partly exposed. Furthermore, coking type particles that appear like snowballs, with diameters in the range of 1–5 μm, are observed at the coking peak section. The reason is that the coking precursor molecules form clusters that appear like snowballs under the action of uniform centrifugal force. The content of element C accumulated at the minor peak is approximately 90%. This part of coking deposition mainly consists of unstable peroxides generated by the ingredient reaction between oxygen and hydrocarbons. From the analysis of the coking characteristics in two different helical tubes, it can be inferred that the effect of centrifugal force is more than that of the number of coils in determining the position of the coking peak; it can also be seen that the coking peak lies closer to the downstream side.

4. Conclusion

Thermal oxidation coking analysis on aviation kerosene RP-3 in four different helical tubes have been conducted by performing experiments with 1 h and 5 h durations at supercritical pressure. Coking distribution, SEM images, and the contents of various elements were discussed for different working conditions, and several related results have been obtained. The results can be summarized as follows.

(1) Centrifugal force inhibits the coking deposition on the inner wall, and no prominent coking peak is observed in the 1 h experiment in helical tubes.
(2) The total coking amount in the experiments with 5 h duration decreased sharply with the increase in the number of helical coils because of the higher centrifugal force. The maximum total coking amount in the helical tubes decreased by approximately 69.5% as compared with that in a straight tube.
(3) Coking precursor is found with three types of coking morphology on the inner surface in different helical tubes: thin coking layer, dense clumps, and crystalline particles.
(4) The results on coking morphology and element percentage could explain the coking deposition at various positions with different distributions of inner wall and bulk temperatures.

References

[1] G. Bruening, W. Chang, Cooled cooling air systems for turbine thermal management, ASME Paper (99-GT) (1999) 14.
[2] D.R. Sobel, L.J. Spadaccini, Hydrocarbon fuel cooling technologies for advanced propulsion, J. Eng. Gas Turb. Power 119 (2) (1997) 344–351.
[3] T. Edwards, S. Zabarnick, Supercritical fuel deposition mechanisms, Ind. Eng. Chem. Res. 32 (12) (1993) 3117–3122.
[4] L.Q. Maurice, H. Lander, T. Edwards, W. Harrison, Advanced aviation fuels: a look ahead via a historical perspective, Fuel 80 (5) (2001) 747–756.
[5] R. Venkataraman, S. Eser, Characterisation of solid deposits from the thermal-oxidative degradation of jet fuel, Int. J. Oil, Gas Coal Technol. 1 (1–2) (2008) 126–137.
[6] S.P. Heneghan, S. Zabarnick, Oxidation of jet fuels and the formation of deposit, Fuel 73 (1) (1994) 35–43.
[7] P. Marteney, L. Spadaccini, Thermal decomposition of aircraft fuel, J. Eng. Gas Turb. Power 108 (4) (1986) 648–653.
[8] R.N. Hazlett, Thermal Oxidation Stability of Aviation Turbine Fuels, ASTM Philadelphia, 1991.
[9] P.A. Masters, C. Aukerman, Deposit formation in hydrocarbon rocket fuels with an evaluation of a propane heat transfer correlation, AIAA Paper 1290 (1982).
[10] E.G. Jones, W.J. Balster, M.E. Post, Degradation of a Jet-A fuel in a single-pass heat exchanger, in: ASME 1993 International Gas Turbine and Aeroengine Congress and Exposition, American Society of Mechanical Engineers, 1993, pp. V03BT16A090.
[11] E.G. Jones, L.M. Balster, W.J. Balster, Autoxidation of neat and blended aviation fuels, Energy Fuels 12 (5) (1998) 990–995.
[12] G.W. Mushrush, E.J. Beal, D.R. Hardy, R.N. Hazlett, D.G. Mose, Liquid phase oxidation of organo-sulfur compounds by tert-butyl hydroperoxide and fuel instability reactions, Fuel 73 (9) (1994) 1481–1485.
[13] R.N. Hazlett, A.J. Power, Phenolic compounds in Bass Strait distillate fuels: their effect on deposit formation, Fuel 68 (9) (1989) 1112–1117.
[14] K. Reddy, W. Roquemore, A time dependent model with global chemistry for decompostition and deposition of aircraft fuels, ACS Paper (90-14) (1990).
[15] A. Ram Mohan, S. Eser, Effectiveness of low-pressure metal–organic chemical vapor deposition coatings on metal surfaces for the mitigation of fouling from heated jet fuel, Ind. Eng. Chem. Res. 50 (12) (2011) 7290–7304.
[16] Y. Wang, G. Xu, H. Deng, X. Luo, Q. Wang, Experimental study of influence of inlet temperature on aviation kerosene coking characteristics, J. Aerospace Power 9 (2009) 1972–1976.
[17] Z. Jia, G. Xu, J. Wen, H. Deng, Experimental study of the influence of surface coke deposition on heat transfer of aviation kerosene RP-3 at supercritical pressure, in: ASME 2012 International Mechanical Engineering Congress and Exposition, American Society of Mechanical Engineers, Houston, Texas, 2012, pp. 1927-1933.
[18] K. Zhu, Z. Tao, G. Xu, Z. Jia, Surface deposition characteristics of supercritical kerosene RP-3 fuel within treated and untreated stainless-steel tubes. Part 1: short thermal duration, Energy Fuels 30 (4) (2016) 2687–2693.
[19] Z. Tao, Y. Fu, G. Xu, H. Deng, Z. Jia, Experimental study on influences of physical factors to supercritical RP-3 surface and liquid-space thermal oxidation coking, Energy Fuels 28 (9) (2014) 6098–6106.
[20] Z. Tao, Y. Fu, G. Xu, H. Deng, Z. Jia, Thermal and element analyses for supercritical RP-3 surface coke deposition under stable and vibration conditions, Energy Fuels 29 (3) (2015) 2006–2013.
[21] X. Pei, L. Hou, Z. Ren, Flow pattern effects on the oxidation deposition rate of aviation kerosene, Energy Fuels 29 (9) (2015) 6088–6094.
[22] Z. Liu, H. Pan, S. Feng, Q. Bi, Dynamic behaviors of coking process during pyrolysis of China aviation kerosene RP-3, App. Therm. Eng. 91 (2015) 408–416.
[23] K. Xu, H. Meng, Numerical study of fluid flows and heat transfer of aviation kerosene with consideration of fuel pyrolysis and surface coking at supercritical pressures, Int. J. Heat Mass Transfer 95 (2016) 806–814.
[24] M. Moawed, Experimental study of forced convection from helical coiled tubes with different parameters, Energy Convers. Manage. 52 (2) (2011) 1150–1156.
[25] Y. Mao, L. Guo, B. Bai, X. Zhang, Convective heat transfer in helical coils for constant-property and variable-property flows with high Reynolds numbers, Front. Energy Power Eng. China 4 (4) (2010) 546–552.

[26] F. Akbaridoust, M. Rakhsha, A. Abbassi, M. Saffar-Avval, Experimental and numerical investigation of nanofluid heat transfer in helically coiled tubes at constant wall temperature using dispersion model, Int. J. Heat Mass Transfer 58 (1–2) (2013) 480–491.
[27] M.H. Kazemi, M.A. Akhavan-Behabadi, M.F. Pakdaman, Pressure Drop and heat transfer characteristics of MWCNT/heat transfer oil nanofluid flow inside microfinned helical tubes with constant wall temperature, Adv. Mater. Res. 622–623 (2012) 796–800.
[28] A. Gomaa, W.I. Aly, M. Omara, M. Abdelmagied, Correlations for heat transfer coefficient and pressure drop in the annulus of concentric helical coils, Heat Mass Transfer 50 (4) (2014) 583–586.
[29] X. Pei, L. Hou, Secondary flow and oxidation coking deposition of aviation fuel, Fuel 167 (2016) 68–74.
[30] H. Deng, C. Zhang, G. Xu, B. Zhang, Z. Tao, K. Zhu, Viscosity measurements of endothermic hydrocarbon fuel from (298 to 788) K under supercritical pressure conditions, J. Chem. Eng. Data 57 (2) (2012) 358–365.
[31] H. Deng, C. Zhang, G. Xu, Z. Tao, K. Zhu, Y. Wang, Visualization Experiments of a Specific Fuel Flow Through Quartz-glass Tubes Under both Sub- and Supercritical Conditions, Chinese J. Aeronaut. 25 (3) (2012) 372–380.
[32] H. Deng, C. Zhang, G. Xu, Z. Tao, B. Zhang, G. Liu, Density measurements of endothermic hydrocarbon fuel at sub-and supercritical conditions, J. Chem. Eng. Data 56 (6) (2011) 2980–2986.
[33] H. Deng, K. Zhu, G. Xu, Z. Tao, C. Zhang, G. Liu, Isobaric specific heat capacity measurement for kerosene RP-3 in the near-critical and supercritical regions, J. Chem. Eng. Data 57 (2) (2011) 263–268.
[34] X. Pei, L. Hou, Effect of dissolved oxygen concentration on coke deposition of kerosene, Fuel Process. Technol. 142 (2016) 86–91.
[35] E. Klavetter, S. Martin, K. Wessendorf, Monitoring jet fuel thermal stability using a quartz crystal microbalance, Energy Fuels 7 (5) (1993) 582–588.
[36] S.P. Heneghan, S.L. Locklear, D.L.I. Geiger, S.D. Anderson, W.D. Schulz, Static tests of jet fuel thermal and oxidative stability, J. Propul. Power 9 (1) (1993) 5–9.
[37] A. Vranos, P.J. Marteney, B.A. Knight, Determination of coking rate in jet fuel, Combust. Sci. Technol. 26 (3–4) (1981) 171–175.
[38] M.Z. Islam, R.N. Mondal, M. Rashidi, Dean-Taylor flow with convective heat transfer through a coiled duct, Comput. Fluids 149 (2017) 41–55.
[39] K.A. Misurati, Y. Quan, W. Gong, G. Xu, Y. Yan, Contrastive study of flow and heat transfer characteristics in a helically coiled tube under uniform heating and one-side heating, App. Therm. Eng. 114 (2017) 77–84.
[40] J. TeVelde, M. Glickstein, Heat Transfer and Thermal Stability of Alternative Aircraft Fuels, US Naval Air Propulsion Center, Trenton, NJ, Report No. NAPC-PE-87C, 1983.
[41] J. Chin, A. Lefebvre, F.-Y. Sun, Temperature effects on fuel thermal stability, J. Eng. Gas Turb. Power 114 (2) (1992) 353–358.
[42] C. Zhang, H. Deng, G. Xu, W. Huang, K. Zhu, Enthalpy measurement and heat transfer investigation of RP-3 kerosene at supercritical pressure, J. Aerospace Power 25 (2) (2010) 331–335.
[43] C. Zhang, G. Xu, L. Gao, Z. Tao, H. Deng, K. Zhu, Experimental investigation on heat transfer of a specific fuel (RP-3) flows through downward tubes at supercritical pressure, J. Supercrit. Fluid 72 (2012) 90–99.
[44] E.F. Schmidt, Wärmeübergang und druckverlust in rohrschlangen, Chemie Ingenieur Technik 39 (13) (1967) 781–789.
[45] R. Venkataraman, S. Eser, Characterization of solid deposits formed from jet fuel degradation under pyrolytic conditions: metal sulfides, Ind. Eng. Chem. Res 47 (23) (2008) 9351–9360.